IOP PUBLISHING CLASSICAL AND QUANTUM GRAVITY

Class. Quantum Grav. **26** (2009) 175006 (12pp) doi:10.1088/0264-9381/26/17/175006

Late-time tails of a self-gravitating massless scalar field, revisited

Piotr Bizoń[1], **Tadeusz Chmaj**[2,3] **and Andrzej Rostworowski**[1]

[1] M Smoluchowski Institute of Physics, Jagiellonian University, Kraków, Poland
[2] H Niewodniczanski Institute of Nuclear Physics, Polish Academy of Sciences, Kraków, Poland
[3] Cracow University of Technology, Kraków, Poland

Received 20 March 2009, in final form 3 June 2009
Published 12 August 2009
Online at stacks.iop.org/CQG/26/175006

Abstract
We discuss the nonlinear origin of the power-law tail in the long-time evolution of a spherically symmetric self-gravitating massless scalar field in even-dimensional spacetimes. Using the third-order perturbation method, we derive explicit expressions for the tail (the decay rate and the amplitude) for solutions starting from small initial data, and we verify this prediction via numerical integration of the Einstein-scalar field equations in four and six dimensions. Our results show that the coincidence of decay rates of linear and nonlinear tails in four dimensions (which has misguided some tail hunters in the past) is in a sense accidental and does not hold in higher dimensions.

PACS numbers: 04.40.Nr, 04.25.Nx

1. Introduction

This paper is concerned with the long-time behavior of a spherically symmetric self-gravitating massless scalar field. This toy-model of gravitational collapse has been intensively studied in the past leading to valuable insights into the validity of the weak cosmic censorship and no-hair conjectures. In particular, Christodoulou proved that there are two generic endstates of evolution: Minkowski spacetime for small initial data [1] and Schwarzschild black hole for large initial data [2]. In both cases, the upper bound for the rate of relaxation to the endstate inside the light cone is t^{-3} (this was proved in [1] for the dispersive solutions and recently by Dafermos and Rodnianski [3] for the collapsing solutions). In view of these rigorous results, one might wonder what is the point of studying this problem again. Our motivation is twofold.

First, it is natural to ask whether the decay rates mentioned above are optimal and, if so, what are the corresponding amplitudes of the tails. This kind of *quantitative* information might be physically relevant (provided that the intuitions gained in this toy-model carry over to more realistic situations), for example, in assessing the possibility of detecting the tails in future gravitational wave experiments.

Second and foremost, we want to clarify some longstanding confusion which is widespread throughout the vast relativity literature dealing with wave tails. To explain what this confusion is about, we need to make some historical remarks. The study of wave tails in general relativity was launched in the seminal paper by Price [4], where he gave a heuristic argument that a linear massless scalar field propagating on the fixed Schwarzschild background decays as t^{-3} near timelike infinity. This result has been later rederived by different methods and confirmed numerically (the works [5–9] are particularly noteworthy), and finally proved rigorously in [3] (as a special decoupled case of the main theorem on the coupled Einstein-scalar system). An especially influential contribution to the study of tails was made in a pair of papers by Gundlach, Price and Pullin [6, 10]. In the first paper, [6], they argued, using linearized theory, that the t^{-3} tail is due to the backscattering of the outgoing radiation off the curvature at large distances, and therefore it is present for any asymptotically flat solution, not only for black hole spacetimes. In the second paper, [10], GPP solved the spherically symmetric Einstein-scalar field equations numerically and found that, indeed, tails do develop for any initial data and moreover they decay as t^{-3} regardless of the endstate of evolution. This work was a significant step toward understanding of tails, however the fact that it appeared back to back with [6] led also (somewhat ironically) to some confusion. Namely, the remarkable agreement between the decay rates of tails observed numerically in the nonlinear evolution [10] and the predictions of the linearized theory [6] has been interpreted (first rather cautiously by the authors themselves and later with increasing sureness in numerous citations of [10]) as if the linearized theory applies qualitatively (and, as long as the power-law exponents of tails are concerned, even quantitatively) in the nonlinear regime. We wish to point out that this interpretation is too naive.

We claim that the tails observed in [10] (and later confirmed in [11, 12] with better numerical accuracy) have genuinely *nonlinear* origin for the dispersive solutions (while for the collapsing solutions they have both linear and nonlinear ingredients). To substantiate our claim, we compute the late-time behavior (the decay rate *and the amplitude* of a tail) of the self-gravitating scalar field in even-dimensional spacetime for small initial data using the nonlinear perturbative scheme developed in our recent papers [13–17]. The outcome of this simple analytic computation is shown to agree extremely well with the results of high-precision numerical integration of the Einstein-scalar field equations in four and six dimensions; however, it does *not* agree with the linearized theory in dimensions higher than 4. Thus, the equality of the decay rates of linear and nonlinear tails seems to be a misleading idiosyncrasy of the Einstein-scalar field equations in four dimensions. This paper is concerned only with subcritical initial data which lead to dispersion. Work on the collapsing solutions is still in progress.

The rest of the paper is organized as follows. In section 2, we construct a simple iterative scheme for solving the spherically symmetric Einstein-scalar field equations in even-dimensional spacetimes. This scheme is applied in section 3 to derive the second-order approximation for the mass function and the third-order approximation for the scalar field in four dimensions. The analogous calculation in higher even dimensions is done in section 4. In section 5, we compare the nonlinear tails with the linear tails on the fixed Schwarzschild background. Section 6 contains numerical evidence confirming the analytic formulae for the tail from sections 3 and 4. In section 7, we make some final remarks.

2. Field equations and the iterative scheme

We consider the self-gravitating real massless scalar field ϕ in $d+1$ dimensions, where $d \geqslant 3$ is odd. The Einstein equations for metric $g_{\alpha\beta}$ are

$$G_{\alpha\beta} = 8\pi T_{\alpha\beta}, \qquad T_{\alpha\beta} = \nabla_\alpha\phi\nabla_\beta\phi - \tfrac{1}{2}g_{\alpha\beta}(\nabla_\mu\phi\nabla^\mu\phi), \tag{1}$$

and the scalar field satisfies the wave equation (which is equivalent to $\nabla_\alpha T^{\alpha\beta} = 0$)

$$\nabla_\mu\nabla^\mu\phi = 0. \tag{2}$$

We assume spherical symmetry, so $\phi = \phi(t, r)$, and use the following ansatz for the metric,

$$\mathrm{d}s^2 = \mathrm{e}^{2\alpha(t,r)}(-\mathrm{e}^{2\beta(t,r)}\,\mathrm{d}t^2 + \mathrm{d}r^2) + r^2\,\mathrm{d}\Omega_{d-1}^2, \tag{3}$$

where $\mathrm{d}\Omega_{d-1}^2$ is the round metric on the unit $(d-1)$-dimensional sphere. We also define the mass function $m(t, r) = (1 - \mathrm{e}^{-2\alpha})r^{d-2}$. In these variables the Einstein equations take the form

$$m' = \kappa r^{d-1}\,\mathrm{e}^{-2\alpha}(\phi'^2 + \mathrm{e}^{-2\beta}\dot\phi^2), \qquad \text{(Hamiltonian constraint)} \tag{4}$$

$$\dot m = 2\kappa r^{d-1}\,\mathrm{e}^{-2\alpha}\dot\phi\phi', \qquad \text{(momentum constraint)} \tag{5}$$

$$\beta' = (d-2)\frac{m}{r^{d-1}}\,\mathrm{e}^{2\alpha}, \tag{6}$$

where $\kappa = \frac{8\pi}{d-1}$, and primes and dots denote partial derivatives with respect to r and t, respectively. Equation (6), corresponding to $G_t^t + G_r^r = 8\pi\left(T_t^t + T_r^r\right) = 0$, is sometimes referred to as the polar slicing condition. The wave equation (2), which can be viewed as the integrability condition for equations (4) and (5), becomes

$$(\mathrm{e}^{-\beta}\dot\phi)^{\cdot} - \frac{1}{r^{d-1}}(r^{d-1}\,\mathrm{e}^{\beta}\phi')' = 0. \tag{7}$$

We assume that initial data are small, smooth and compactly supported (the last assumption can be replaced by a suitable fall-off condition)

$$\phi(0, r) = \varepsilon f(r), \qquad \dot\phi(0, r) = \varepsilon g(r). \tag{8}$$

We make the following perturbative expansion:

$$m(t, r) = m_0(t, r) + \varepsilon m_1(t, r) + \varepsilon^2 m_2(t, r) + \cdots, \tag{9}$$

$$\beta(t, r) = \beta_0(t, r) + \varepsilon\beta_1(t, r) + \varepsilon^2\beta_2(t, r) + \cdots, \tag{10}$$

$$\phi(t, r) = \phi_0(t, r) + \varepsilon\phi_1(t, r) + \varepsilon^2\phi_2(t, r) + \varepsilon^3\phi_3(t, r) + \cdots. \tag{11}$$

Substituting this expansion into the field equations and grouping terms with the same power of ε, we get the iterative scheme which can be solved recursively.

In this paper we consider perturbations about Minkowski spacetime, so $m_0 = \beta_0 = \phi_0 = 0$. At the first order the metric functions $m_1 = \beta_1 = 0$ (this follows from regularity at $r = 0$), while ϕ_1 satisfies the flat space radial wave equation $\left(\Box = \partial_t^2 - \partial_r^2 - \frac{d-1}{r}\partial_r\right)$

$$\Box\phi_1 = 0, \qquad \phi_1(0, r) = f(r), \qquad \dot\phi_1(0, r) = g(r). \tag{12}$$

The general spherically symmetric solution of equation (12) in odd spatial dimensions $d = 2\ell + 3$ is given by a superposition of outgoing and ingoing waves

$$\phi_1(t, r) = \phi_1^{\mathrm{ret}}(t, r) + \phi_1^{\mathrm{adv}}(t, r), \tag{13}$$

where

$$\begin{aligned}
\phi_1^{\mathrm{ret}}(t, r) &= \frac{1}{r^{\ell+1}}\sum_{k=0}^{l}\frac{(2\ell-k)!}{k!(\ell-k)!}\frac{a^{(k)}(u)}{(v-u)^{\ell-k}},\\
\phi_1^{\mathrm{adv}}(t, r) &= \frac{1}{r^{\ell+1}}\sum_{k=0}^{\ell}(-1)^{k+1}\frac{(2\ell-k)!}{k!(\ell-k)!}\frac{a^{(k)}(v)}{(v-u)^{\ell-k}},
\end{aligned} \tag{14}$$

and $u = t - r$, $v = t + r$ are the retarded and advanced times, respectively (the superscript in round brackets denotes the kth derivative). Note that for compactly supported initial data, the generating function $a(x)$ can be chosen to have compact support as well (this condition determines $a(x)$ uniquely).

At the second order $\Box\phi_2 = 0$, hence $\phi_2 = 0$ (because it has zero initial data), while the metric functions satisfy the following equations:

$$m_2' = \kappa r^{d-1}\left(\dot\phi_1^2 + \phi_1'^2\right), \tag{15}$$

$$\dot m_2 = 2\kappa r^{d-1}\dot\phi_1\phi_1', \tag{16}$$

$$\beta_2' = \frac{(d-2)m_2}{r^{d-1}}. \tag{17}$$

We postpone the discussion of this system to the following section and now proceed to the third order, where we have

$$\Box\phi_3 = 2\beta_2\ddot\phi_1 + \dot\beta_2\dot\phi_1 + \beta_2'\phi_1'. \tag{18}$$

To solve this equation we use the Duhamel formula for the solution of the inhomogeneous wave equation $\Box\phi = N(t,r)$ with zero initial data

$$\phi(t,r) = \frac{1}{2r^{\ell+1}}\int_0^t \mathrm{d}\tau \int_{|t-r-\tau|}^{t+r-\tau} \rho^{\ell+1} P_\ell(\mu) N(\tau,\rho)\,\mathrm{d}\rho, \tag{19}$$

where $P_\ell(\mu)$ are Legendre polynomials of degree ℓ (recall that $\ell = (d-3)/2$) and $\mu = (r^2+\rho^2-(t-\tau)^2)/2r\rho$ (note that $-1 \leqslant \mu \leqslant 1$ within the integration range). Applying this formula to equation (18), using null coordinates $\eta = \tau - \rho$ and $\xi = \tau + \rho$, and the abbreviation $K(\beta,\phi) = 2\beta\ddot\phi + \dot\beta\dot\phi + \beta'\phi'$, we obtain

$$\phi_3(t,r) = \frac{1}{2^{\ell+3}r^{\ell+1}}\int_{|t-r|}^{t+r}\mathrm{d}\xi\int_{-\xi}^{t-r}(\xi-\eta)^{\ell+1}P_\ell(\mu)K(\beta_2(\xi,\eta),\phi_1(\xi,\eta))\,\mathrm{d}\eta, \tag{20}$$

where now $\mu = (r^2+(\xi-t)(t-\eta))/r(\xi-\eta)$. If the initial data (8) vanish outside a ball of radius R, then for $t > r + R$ we may drop the advanced part of $\phi_1(t,r)$ and interchange the order of integration in (20) to get

$$\phi_3(t,r) = \frac{1}{2^{\ell+3}r^{\ell+1}}\int_{-\infty}^{\infty}\mathrm{d}\eta\int_{t-r}^{t+r}(\xi-\eta)^{\ell+1}P_\ell(\mu)K(\beta_2(\xi,\eta),\phi_1^{\mathrm{ret}}(\xi,\eta))\,\mathrm{d}\xi. \tag{21}$$

In order to determine the behavior of $\phi_3(t,r)$ for large t, we need only to know the behavior of the metric function $\beta_2(t,r)$ along the light cone for large values of r (the intersection of the integration range in (21) with the support of $\phi_1^{\mathrm{ret}}(t,r)$). This calculation will be done in the following section. Having that, we shall expand the function K in (21) in the inverse powers of $(\xi-\eta)$ and use the identity (see the appendix in [16] for the derivation)

$$\int_{t-r}^{t+r}\mathrm{d}\xi\,\frac{P_\ell(\mu)}{(\xi-\eta)^n} = (-1)^\ell\frac{2(n-2)^{\underline{\ell}}}{(2\ell+1)!!}\frac{r^{\ell+1}(t-\eta)^{n-\ell-2}}{[(t-\eta)^2-r^2]^{n-1}}F\left(\begin{matrix}\frac{\ell+2-n}{2},\frac{\ell+3-n}{2}\\ \ell+3/2\end{matrix}\,\middle|\,\left(\frac{r}{t-\eta}\right)^2\right), \tag{22}$$

where $(n-2)^{\underline{\ell}} = (n-2)(n-3)\cdots(n-\ell-1)$ $(\ell > 0)$ and $(n-2)^{\underline{0}} = 1$.

If one has no fear, this iterative procedure can be continued to higher orders; however, it seems like an overkill in view of two facts. First, the iteration has no chance to converge (cf [18]) so our perturbation series is only asymptotic. Second, already the third-order approximation shows perfect agreement with numerical results (see section 6).

3. Nonlinear tail in 3 + 1 dimensions

In this section, written mainly for the benefit of the reader who is not interested in higher dimensions, we follow the general strategy sketched above to present a detailed calculation of the third-order iterate $\phi_3(t,r)$ in three spatial dimensions. In the following section we shall repeat this calculation for any odd spatial dimension $d \geqslant 3$.

For $d = 3$ (hence $l = 0$), the solution (13), (14) of the free wave equation takes the form

$$\phi_1(t,r) = \frac{a(u) - a(v)}{r}, \tag{23}$$

where the function $a(x)$ is uniquely determined by the initial data. Substituting (23) into (15) and integrating, we get

$$m_2(t,r) \overset{t\geq R}{=} 4\pi \int_0^r \left(2a'^2(t-\rho) - \partial_\rho \frac{a^2(t-\rho)}{\rho}\right) \mathrm{d}\rho, \tag{24}$$

where we used that $m_2(t, r = 0) = 0$, which follows from regularity of initial data at the origin and (16). Here and in the following we use repeatedly the fact that $a(x) = 0$ for $|x| > R$, R being the radius of a ball on which the initial data (8) are supported. To describe the behavior of $m_2(t,r)$ near the lightcone, it is convenient to use the null coordinate $u = t - r$ instead of t, and rewrite (24) as

$$m_2(u,r) \overset{r+u\geq R}{=} 4\pi \left(2\int_u^\infty a'^2(s)\,\mathrm{d}s - \frac{a^2(u)}{r}\right). \tag{25}$$

Next, using the gauge freedom to set $\beta_2(t, r = 0) = 0$ and integrating equation (17), we get

$$\beta_2(t,r) \overset{t\geq R}{=} 4\pi \left(2\int_0^r \frac{1}{\rho^2}\int_{t-\rho}^\infty a'^2(s)\,\mathrm{d}s\,\mathrm{d}\rho - \int_0^r \frac{a^2(t-\rho)}{\rho^3}\,\mathrm{d}\rho\right). \tag{26}$$

The first integral can be integrated by parts giving

$$\beta_2(u,r) \overset{r+u\geq R}{=} 4\pi \left(-\frac{2}{r}\int_u^\infty a'^2(s)\,\mathrm{d}s + 2\int_u^\infty \frac{a'^2(s)}{r-(s-u)}\,\mathrm{d}s - \int_u^\infty \frac{a^2(s)}{(r-(s-u))^3}\,\mathrm{d}s\right). \tag{27}$$

In order to determine the tail of ϕ_3, we need only two leading terms in the expansion of the above formula in the inverse powers of r. Hereafter, it is convenient to define the following integrals (for non-negative integers m, n):

$$I_n^m(u) = \int_u^\infty (s-u)^m \left(a^{(n)}(s)\right)^2 \mathrm{d}s. \tag{28}$$

Then our results can be cast in the form

$$\beta_2(u,r) \overset{r+u\geq R}{=} \frac{4\pi}{r^2}\left[2I_1^1(u) + \frac{1}{r}\left(2I_1^2(u) - I_0^0(u)\right) + \mathcal{O}\left(\frac{1}{r^2}\right)\right], \tag{29}$$

$$\dot\beta_2(u,r) \overset{r+u\geq R}{=} -\frac{4\pi}{r^2}\left[2I_1^0(u) + \frac{1}{r}\left(4I_1^1(u) - a^2(u)\right) + \mathcal{O}\left(\frac{1}{r^2}\right)\right], \tag{30}$$

$$\beta_2'(u,r) \overset{r+u\geq R}{=} \frac{4\pi}{r^2}\left[2I_1^0(u) - \frac{1}{r}a^2(u) + \mathcal{O}\left(\frac{1}{r^2}\right)\right]. \tag{31}$$

Substituting (23) and (29)–(31) into (21) (with $\ell = 0$) we get for $t > r + 3R$

$$\phi_3(t,r) = \frac{2^4\pi}{r}\int_{-\infty}^{+\infty}\mathrm{d}\eta\int_{t-r}^{t+r}\frac{\mathrm{d}\xi}{(\xi-\eta)^2} \times\left[\frac{d}{\mathrm{d}\eta}\left(I_1^1(\eta)a'(\eta)\right) + \frac{1}{\xi-\eta}\left(I_1^0(\eta)a(\eta) + \frac{d}{\mathrm{d}\eta}Q_0(\eta)\right) + \mathcal{O}\left(\frac{1}{(\xi-\eta)^2}\right)\right], \tag{32}$$

where

$$Q_0(\eta) = 2I_1^1(\eta)a(\eta) + \big(2I_1^2(\eta) - I_0^0(\eta)\big)a'(\eta). \tag{33}$$

Elementary integrations over ξ and by parts over η yield for large retarded times $u = t - r$

$$\phi_3(t,r) = \frac{t}{(t^2-r^2)^2}\left[\Gamma_0 + \mathcal{O}\left(\frac{t}{t^2-r^2}\right)\right], \tag{34}$$

where the coefficient

$$\Gamma_0 = -2^5\pi \int_{-\infty}^{+\infty} I_1^0(s)a(s)\,\mathrm{d}s \tag{35}$$

is the only trace of initial data. From (34) we obtain the late-time tails in two asymptotic regimes: $\phi_3(t,r) \simeq \Gamma_0 t^{-3}$ at future timelike infinity ($r = \text{const}, t \to \infty$) and $(r\phi_3)(v = \infty, u) \simeq \frac{1}{4}\Gamma_0 u^{-2}$ at future null infinity ($v = \infty, u \to \infty$).

4. Nonlinear tail in $d + 1$ dimensions

Proceeding along the same lines as described in detail in the previous section, we get the analogs of formulae (29)–(31) in $d + 1$ dimensions (recall that $d = 2\ell + 3$ so $\kappa = 4\pi/(\ell + 1)$)

$$\beta_2(u,r) \overset{r+u>R}{=} \frac{(2\ell+1)\kappa}{r^{2\ell+2}}\left[2I_{\ell+1}^1(u) + \frac{\ell+1}{r}\left(2I_{\ell+1}^2(u) - (\ell+1)I_\ell^0(u)\right) + \mathcal{O}\left(\frac{1}{r^2}\right)\right], \tag{36}$$

$$\dot\beta_2(u,r) \overset{r+u>R}{=} -\frac{(2\ell+1)\kappa}{r^{2\ell+2}}\left[2I_{\ell+1}^0(u) + \frac{\ell+1}{r}\left(4I_{\ell+1}^1(u) - (\ell+1)(a^{(\ell)}(u))^2\right) + \mathcal{O}\left(\frac{1}{r^2}\right)\right], \tag{37}$$

$$\beta_2'(u,r) \overset{r+u>R}{=} \frac{(2\ell+1)\kappa}{r^{2\ell+2}}\left[2I_{\ell+1}^0(u) - (\ell+1)^2\frac{1}{r}\left(a^{(\ell)}(u)\right)^2 + \mathcal{O}\left(\frac{1}{r^2}\right)\right], \tag{38}$$

with $I_n^m(u)$ defined in (28). Substituting these expressions into (21) we get for $t > r + 3R$

$$\begin{aligned}\phi_3(t,r) = \frac{2^{2\ell+2}(2\ell+1)\kappa}{r^{\ell+1}}\int_{-\infty}^{+\infty}\mathrm{d}\eta\int_{t-r}^{t+r}\frac{\mathrm{d}\xi}{(\xi-\eta)^{2\ell+2}}\Bigg[\frac{d}{\mathrm{d}\eta}\left(I_{\ell+1}^1(\eta)a^{(\ell+1)}(\eta)\right)\\ + \frac{\ell+1}{\xi-\eta}\left(I_{\ell+1}^0(\eta)a^{(\ell)}(\eta) + \frac{d}{\mathrm{d}\eta}Q_\ell(\eta)\right) + \mathcal{O}\left(\frac{1}{(\xi-\eta)^2}\right)\Bigg],\end{aligned} \tag{39}$$

where

$$Q_\ell(\eta) = (\ell+2)I_{\ell+1}^1(\eta)a^{(\ell)}(\eta) + \big(2I_{\ell+1}^2(\eta) - (\ell+1)I_0^0(\eta)\big)\,a^{(\ell+1)}(\eta). \tag{40}$$

Using the identity (22) we get the asymptotic behavior for large retarded times $u = t - r$

$$\begin{aligned}\phi_3(t,r) = \frac{t^{\ell+1}}{(t^2-r^2)^{2\ell+2}}\Bigg\{\left(4\ell+2-\ell\left(1-\frac{r^2}{t^2}\right)\right)F\left(\begin{matrix}-\frac{\ell}{2},-\frac{\ell}{2}+\frac{1}{2}\\ \ell+3/2\end{matrix}\,\middle|\,\frac{r^2}{t^2}\right)\\ - (2\ell+1)F\left(\begin{matrix}-\frac{\ell}{2},-\frac{\ell}{2}-\frac{1}{2}\\ \ell+3/2\end{matrix}\,\middle|\,\frac{r^2}{t^2}\right)\Bigg\}\left[\frac{\Gamma_\ell}{\ell+1} + \mathcal{O}\left(\frac{t}{t^2-r^2}\right)\right],\end{aligned} \tag{41}$$

where

$$\Gamma_\ell = (-1)^{l+1}2^{3l+5}\pi\int_{-\infty}^{+\infty} I_{\ell+1}^0(s)a^{(\ell)}(s)\,\mathrm{d}s. \tag{42}$$

For $\ell = 0$, the formula (41) reduces to (34). For $\ell \geqslant 1$, the integral (42) can be integrated by parts again, giving

$$\Gamma_\ell = (-1)^{l+1}2^{3l+5}\pi\int_{-\infty}^{+\infty}(a^{(\ell+1)}(s))^2a^{(\ell-1)}(s)\,\mathrm{d}s. \tag{43}$$

Asymptotics at time and null infinity are easily obtained from (41). They read

$$\phi_3(t,r) = \frac{1}{t^{3\ell+3}}\left[\Gamma_\ell + \mathcal{O}\left(\frac{1}{t}\right)\right], \tag{44}$$

$$(r^{\ell+1}\phi_3)(v=\infty,u) = \frac{1}{u^{2\ell+2}}\left[\frac{(2\ell+1)!(2\ell+1)!!}{2(3\ell+2)!}\Gamma_\ell + \mathcal{O}\left(\frac{1}{u}\right)\right]. \tag{45}$$

This is our main result. We claim that the formulae (44) and (45) provide very good approximations of the tail for solutions with sufficiently small initial data. By this we mean that for any given smooth compactly supported profiles $f(r)$ and $g(r)$ in (8), one can choose ε so small that

$$\lim_{t\to\infty} t^{3\ell+3}|\phi(t,r) - \varepsilon^3\phi_3(t,r)| = \mathcal{O}(\varepsilon^5), \tag{46}$$

$$\lim_{u\to\infty} u^{2\ell+2}|(r^{\ell+1}(\phi - \varepsilon^3\phi_3))(v=\infty,u))| = \mathcal{O}(\varepsilon^5), \tag{47}$$

at time and null infinity, respectively. Numerical evidence for this claim is given in section 6.

5. Linear scalar waves on Schwarzschild background

For the sake of completeness, in this section we recall briefly what is known about the decay of the massless scalar field propagating outside the $(d+1)$-dimensional Schwarzschild black hole

$$\mathrm{d}s^2 = -\left(1 - \frac{M}{r^{d-2}}\right)\mathrm{d}t^2 + \left(1 - \frac{M}{r^{d-2}}\right)^{-1}\mathrm{d}r^2 + r^2\,\mathrm{d}\Omega_{d-1}^2. \tag{48}$$

As above, we consider only odd spatial dimensions $d \geqslant 3$ and use the integer index $\ell = (d-3)/2$. In terms of the tortoise coordinate x, defined by $\mathrm{d}r/\mathrm{d}x = 1 - M/r^{2\ell+1}$, and the variable $\psi(x) = r^{\ell+1}\phi(r)$, the radial wave equation in the metric (48) for $r \geqslant M$ reduces to the flat spacetime $(1+1)$-dimensional wave equation with the potential (on the whole axis $-\infty < x < \infty$)

$$\partial_t^2\psi - \partial_x^2\psi + V(x)\psi = 0, \qquad V = \left(1 - \frac{M}{r^{2\ell+1}}\right)\left(\frac{\ell(\ell+1)}{r^2} + \frac{M(\ell+1)^2}{r^{2\ell+3}}\right). \tag{49}$$

Now, there is an important difference between $\ell = 0$ and $\ell > 0$ cases which is due to the fact that only for $\ell = 0$ the tortoise coordinate involves the logarithm. More concretely, for $\ell = 0$ we have

$$x = r + M\ln(r/M - 1), \tag{50}$$

hence for $x \gg M$

$$r = x - M\ln(x/M) + \frac{M^2\ln(x/M)}{x} + \frac{M^2}{x} + \mathcal{O}\left(\frac{M^3\ln^2(x/M)}{x^2}\right), \tag{51}$$

and therefore

$$V(x) = \frac{M}{x^3} + \frac{3M^2\ln(x/M)}{x^4} - \frac{M^2}{x^4} + \mathcal{O}\left(\frac{M^3\ln^2(x/M)}{x^5}\right), \tag{52}$$

which gives rise to the Price tail $\phi(t,r) \sim Mt^{-3}$ [4].

In contrast, for $\ell \geqslant 1$ we have (see [15])

$$r = x + \frac{1}{2\ell}\frac{M}{x^{2\ell}} - \frac{2\ell+1}{2\ell(4\ell+1)}\frac{M^2}{x^{4\ell+1}} + \mathcal{O}\left(\frac{M^3}{x^{6\ell+2}}\right), \tag{53}$$

which implies that for large x

$$V(x) = \frac{\ell(\ell+1)}{x^2} + \frac{(2\ell+1)^2(\ell+1)(4\ell+3)}{4\ell(4\ell+1)}\frac{M^2}{x^{4\ell+4}} + \mathcal{O}\left(\frac{M^3}{x^{6\ell+5}}\right). \tag{54}$$

A remarkable feature of this effective potential is the absence of a term proportional to M. It is for this reason that the tail drops very rapidly:

$$\phi(t, r) \sim \frac{M^2}{t^{6\ell+4}}, \tag{55}$$

as follows from the general formula $t^{-(\alpha+2\ell)}$ for the tail produced by the potential of the form $\ell(\ell+1)/x^2 + U(x)$ with $U(x) \sim x^{-\alpha}$ for large x [7, 15].

6. Numerics

In order to verify the above analytic predictions, we solved numerically the initial value problem (4)–(8) for various initial data. To this end, we rewrite the wave equation (7) as a pair of two first-order equations for auxiliary fields $\Phi = \phi'$ and $\Pi = \mathrm{e}^{-\beta}\dot{\phi}$:

$$\dot{\Pi} = \frac{1}{r^{d-1}}(r^{d-1}\,\mathrm{e}^{\beta}\Phi)' \quad \text{and} \quad \dot{\Phi} = (\mathrm{e}^{\beta}\Pi)'. \tag{56}$$

We solve these equations with fourth-order accurate Runge–Kutta time stepping using finite differencing in space. At each time step we update the metric functions $m(t, r)$ and $\beta(t, r)$ by integrating the Hamiltonian constraint (4) and the slicing condition (6) with the fourth-order Runge–Kutta method. To ensure regularity at the origin we impose the boundary conditions $\Phi(t, 0) = 0$ and $\Pi'(t, 0) = 0$, which are implemented by $\Phi(t, r)$ and $\Pi(t, r)$ being odd and even functions of r, respectively. To avoid the contamination of the tail by spurious reflections from the outer boundary of the computational grid, we place that boundary far away and compute the solution only inside the domain of dependence of the initial surface. As was pointed out in [7], a reliable numerical computation of tails requires high-order finite difference schemes, since otherwise the ghost potentials generated by discretization errors produce artificial tails which might mask the genuine behavior. We used fourth- and tenth-order difference schemes for $d = 3$ and $d = 5$ dimensions, respectively[4]. To eliminate high-frequency numerical instabilities, we add a small amount of artificial dissipation [19], that is, after each time step advancing solution f from t to $t + \Delta t$ on a grid with $(\Delta t, \Delta r)$ mesh we add the Kreiss–Oliger dissipative term $f(t + \Delta t, r) \longrightarrow f(t + \Delta t, r) + Q_k f(t, r)$, where (for consistency with $2(k-1)$-order finite difference scheme) Q_k is a finite-difference operator of order $2k$ of form $Q_k = (-1)^{k+1}\frac{\sigma}{2^{2k}}\left(\frac{\Delta t}{\Delta r}\right)(\Delta_+)^k(\Delta_-)^k$ where σ is of order 1 and $\Delta_\pm f(t, r) = \pm(f(t, r \pm \Delta r) - f(t, r))$. Finally, to suppress the accumulation of round-off errors at late times our codes were run in 128 bit precision. For the above reasons the accurate numerical simulations of tails, albeit straightforward, are computationally expensive even in spherical symmetry.

[4] On the fixed Schwarzschild background in $d = 5$, the scalar field $\phi(t, r)$ decays as t^{-10} (see (55)). If a weak self-gravitating scalar field decayed at this rate, its tail would be hidden under an artificial tail generated by a ghost potential unless the tenth or higher order discretization is used.

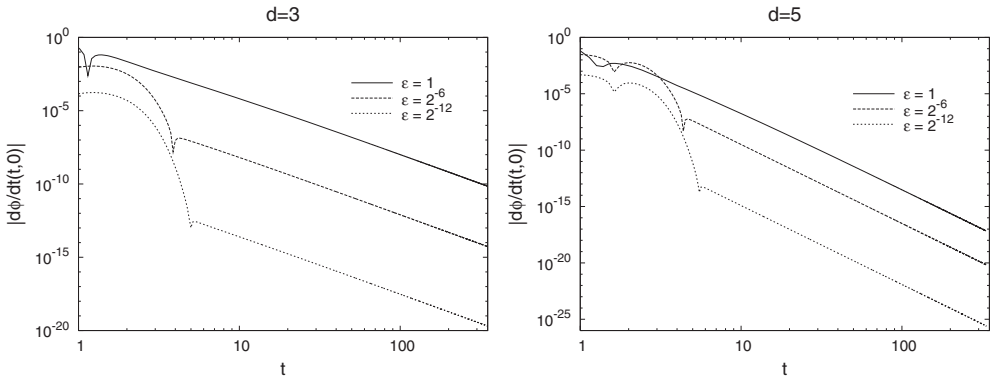

Figure 1. The log–log plot of $\dot\phi(t,0)$ for small ($\varepsilon = 2^{-12}$), intermediate ($\varepsilon = 2^{-6}$) and large ($\varepsilon = 1$) amplitudes of initial data. The slopes ($\gamma = 4$ for $d = 3$ and $\gamma = 7$ for $d = 5$) do not depend on the size of the data.

The numerical results presented here correspond to initial data generated by the function (see (14))

$$\varepsilon a(x) = \frac{\varepsilon}{\sqrt{2\pi}} \exp(-x^2) \tag{57}$$

for different values of ε. For these initial data, our third-order approximation (44) yields the following asymptotic behavior at timelike infinity:

$$\dot\phi(t,r) = 12\sqrt{\pi}\varepsilon^3 \frac{1}{t^4}\left(1 + \mathcal{O}\left(\frac{1}{t}\right)\right) \qquad \text{for} \quad d = 3 \tag{58}$$

and

$$\dot\phi(t,r) = -\frac{1024\sqrt{2}\varepsilon^3}{\sqrt{3}} \frac{1}{t^7}\left(1 + \mathcal{O}\left(\frac{1}{t}\right)\right) \qquad \text{for} \quad d = 5. \tag{59}$$

In figure 1 we plot $\dot\phi(t,0) = \mathrm{e}^{\beta}\Pi(t,0)$ in $d = 3$ and $d = 5$ for three different values of ε. The late-time tails are clearly seen as straight lines on log–log plots. We fit our numerical data with the formula

$$\dot\phi(t,r) = At^{-\gamma}\exp(B/t + C/t^2), \tag{60}$$

which gives the local power index (LPI) [11]

$$n(t,r) := -t\ddot\phi(t,r)/\dot\phi(t,r) = \gamma + B/t + 2C/t^2. \tag{61}$$

We plot the local power index at $r = 0$ as a function of $1/t$ in figure 2.

Our fitting procedure proceeds in two steps. First, from the local power index data on the interval $0 < 1/t < 1/50$ we fit γ, B and C in (61). Next, having determined γ, B and C in this way, we fit A in (60) from $\dot\phi$ data on the interval $t > 50$. We have verified that the outcome of the fit (the amplitude A and the decay rate γ) does not depend on the observation point r. The results for $r = 0$ and their confrontation with analytic predictions are summarized in table 1 for $d = 3$ and table 2 for $d = 5$. The agreement between our third-order approximation and the results of numerical integration of the Einstein-scalar field equations is excellent for sufficiently small initial data.

In figure 3 we plot the fitted amplitude of the tail versus the amplitude of initial data and compare it with our third-order analytic formula. The deviation from the scaling $A \sim \varepsilon^3$ for

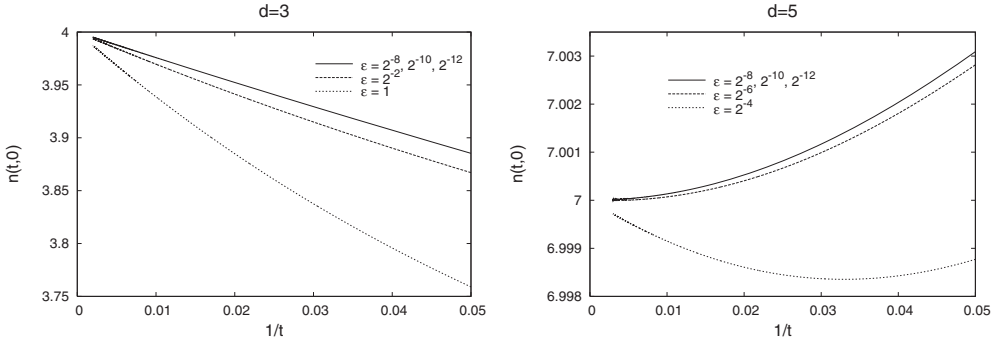

Figure 2. The local power index $n(t, 0)$ as a function of $1/t$. The curves corresponding to small initial data ($\varepsilon = 2^{-8}, 2^{-10}, 2^{-12}$) are indistinguishable which indicates that higher order corrections in the perturbation series are negligible.

Table 1. $d = 3$.

	Numerics: LPI data			Theory (third order)		Numerics: $\dot{\phi}$ data
ε	B	C	γ	γ	A	A
2^{-12}	−2.453 84	1.981 80	4.0000	4	$3.095\,11 \times 10^{-10}$	$3.095\,11 \times 10^{-10}$
2^{-10}	−2.449 83	1.713 98	4.0000	4	$1.980\,87 \times 10^{-8}$	$1.980\,83 \times 10^{-8}$
2^{-8}	−2.449 77	1.698 14	4.0000	4	$1.267\,76 \times 10^{-6}$	$1.267\,60 \times 10^{-6}$
2^{-6}	−2.452 70	1.712 75	4.0000	4	$8.113\,65 \times 10^{-5}$	$8.099\,71 \times 10^{-5}$
2^{-4}	−2.499 38	1.958 63	4.0000	4	$5.192\,74 \times 10^{-3}$	$5.053\,55 \times 10^{-3}$
2^{-3}	−2.642 86	2.708 11	4.0000	4	0.041 5419	0.037 3293
2^{-2}	−3.141 14	5.244 92	4.0000	4	0.332 335	0.222 460
2^{-1}	−4.425 97	11.2084	4.0000	4	2.658 68	0.737 111
1	−6.496 35	18.7893	3.9999	4	21.2694	1.073 16
2	−8.989 50	25.4951	4.0002	4	170.156	0.997 247
4	−11.8828	32.3576	4.0021	4	1361.24	0.892 345

Table 2. $d = 5$.

	Numerics: LPI data			Theory (third order)		Numerics: $\dot{\phi}$ data
ε	B	C	γ	γ	A	A
2^{-12}	$4.642\,90 \times 10^{-4}$	0.650 257	7.0000	7	$-1.216\,67 \times 10^{-8}$	$-1.216\,67 \times 10^{-8}$
2^{-10}	$2.485\,54 \times 10^{-4}$	0.654 252	7.0000	7	$-7.786\,72 \times 10^{-7}$	$-7.786\,44 \times 10^{-7}$
2^{-8}	$-1.024\,40 \times 10^{-4}$	0.654 138	7.0000	7	$-4.983\,50 \times 10^{-5}$	$-4.980\,72 \times 10^{-5}$
2^{-6}	$-6.106\,26 \times 10^{-3}$	0.660 806	7.0000	7	$-3.189\,44 \times 10^{-3}$	$-3.161\,23 \times 10^{-3}$
2^{-4}	−0.100 262	0.765 030	7.0000	7	−0.204 124	−0.177 845
2^{-3}	−0.380 511	1.071 74	7.0000	7	−1.632 99	−0.986 771
2^{-2}	−1.288 78	2.052 37	7.0000	7	−13.0639	−2.825 27
2^{-1}	−3.482 34	4.295 13	7.0000	7	−104.512	−3.537 01
1	−6.866 34	7.068 40	7.0000	7	−836.092	−3.256 61

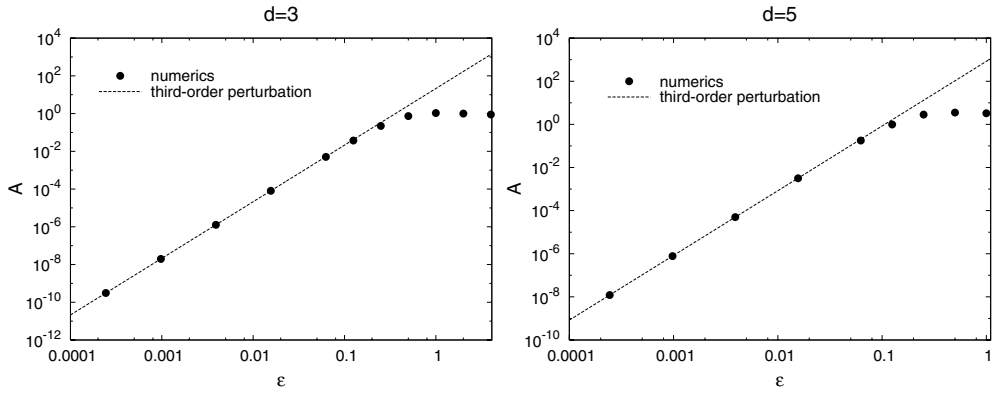

Figure 3. The log–log plot of the amplitude of the tail as a function of the amplitude of initial data (black dots). The third-order approximation (dashed line) is excellent for small data, but it deteriorates for large data lying near the threshold for black hole formation ($\varepsilon \sim 1$). The scaling $A \sim \varepsilon^3$ was previously observed by GPP (see figure 14 in [10]).

large ε signals the breakdown of the third-order approximation. We stress that we get the same decay rates ($\gamma = 4$ for $d = 3$ and $\gamma = 7$ for $d = 5$) for all subcritical evolutions, regardless of whether our third-order formula predicts correctly the amplitude of the tail (for small data) or fails (for large data where higher order terms in the asymptotic expansion (11) cannot be neglected).

7. Final remarks

Using the third-order perturbation method we derived explicit formulae for the late-time tail (the decay rate *and* the amplitude) of a spherically symmetric, self-gravitating massless scalar field for solutions starting from small initial data. We verified that these formulae are in excellent agreement with the results of numerical integration of the Einstein-scalar field equations in four and six dimensions. Our results show that the tail has genuinely *nonlinear* origin and should not be mistaken with the linear tail coming from the backscattering off the Schwarzschild potential. It seems to us that this distinction between linear and nonlinear tails has not been widely recognized in the past which is probably due to the fact that in four-dimensional spacetimes these two different tails decay at the same rate t^{-3}. To demonstrate that this coincidence is an idiosyncrasy of four dimensions, we computed both kinds of tails in $d + 1$ dimensions for $d = 2\ell + 3$ ($\ell = 1, 2, \ldots$) and showed that the linear and nonlinear tails decay at different rates: $t^{-(6\ell+4)}$ and $t^{-(3\ell+3)}$, respectively. This illustrates how viewing the dimension of a spacetime as a parameter may help understand which features of general relativity depend crucially on our world being four dimensional and which ones are general.

It would be interesting to generalize the results of this paper to collapsing solutions where the endstate of evolution is a black hole. The studies in this direction are in progress and will be reported elsewhere. We expect that in this case the tail has both linear and nonlinear contributions with the latter being qualitatively the same as for dispersive solutions described above. Note that the analogous perturbative calculation of tails is much harder on the black hole background because two basic tools that we used above, Huygens' principle and the explicit expression for Duhamel's formula, are missing. For dispersive solutions these tools allowed us to compute the third-order perturbation in a shamelessly explicit way; however,

from the perspective of generalizing the results to collapsing solutions, it is instructive to redo this calculation in an asymptotic manner keeping track of only leading order terms in the perturbative equations. Such an efficient calculation, which gives additional insight into the mechanism of some cancellations in our asymptotic expansions, has been done recently by Szpak [20] and will appear as a comment on this paper.

Acknowledgments

We would like to thank Nikodem Szpak for valuable discussions. We acknowledge support by the MNII grants: NN202 079235 and 189/6.PRUE/2007/7. PB is grateful to Albert Einstein Institute in Golm and Mittag-Leffler Institute in Djursholm for hospitality during part of work on this paper.

References

[1] Christodoulou D 1986 *Commun. Math. Phys.* **105** 337
[2] Christodoulou D 1991 *Commun. Pure Appl. Math.* **44** 339
[3] Dafermos M and Rodnianski I 2005 *Invent. Math.* **162** 381
[4] Price R H 1972 *Phys. Rev.* D **5** 2419
[5] Leaver E W 1986 *Phys. Rev.* D **34** 384
[6] Gundlach C, Price R and Pullin J 1994 *Phys. Rev.* D **49** 883
[7] Ching E S C *et al* 1995 *Phys. Rev.* D **52** 2118
[8] Barack L 1999 *Phys. Rev.* D **59** 044017
[9] Pürer M, Husa S and Aichelburg P C 2005 *Phys. Rev.* D **71** 104005
[10] Gundlach C, Price R and Pullin J 1994 *Phys. Rev.* D **49** 890
[11] Burko L M and Ori A 1997 *Phys. Rev.* D **56** 7820
[12] Marsa R L and Choptuik M W 1996 *Phys. Rev.* D **54** 4929
[13] Bizoń P, Chmaj T and Rostworowski A 2007 *Phys. Rev.* D **75** 121702
[14] Bizoń P, Chmaj T and Rostworowski A 2007 *Class. Quantum Grav.* **24** F55
[15] Bizoń P, Chmaj T and Rostworowski A 2007 *Phys. Rev.* D **76** 124035
[16] Bizoń P, Chmaj T and Rostworowski A 2008 *Phys. Rev.* D **78** 024044
[17] Szpak N *et al* 2009 *J. Hyperbolic Diff. Eqns* **6** 107
[18] Rendall A D 1990 *Class. Quantum Grav.* **7** 803
[19] Kreiss H O and Oliger J 1973 *Methods for the Approximate Solution of Time Dependent Problems (GARP Publication Series* vol 10*)* (Geneva: World Meteorological Organization)
[20] Szpak N 2009 arXiv:0907.5146